J Mol Model (2013) 19:305–314
DOI 10.1007/s00894-012-1547-4

ORIGINAL PAPER

Periodic density functional theory study of the high-pressure behavior of energetic crystalline 1,4-dinitrofurazano[3, 4-b]piperazine

Wentao Wang · Weihua Zhu · Jinshan Li · Bibo Cheng · Heming Xiao

Received: 15 June 2012 / Accepted: 23 July 2012 / Published online: 14 August 2012

Abstract A detailed study of the structural, electronic, and optical absorption properties of crystalline 1,4-dinitrofurazano[3,4-b]piperazine (DNFP) under hydrostatic pressures of 0–100 GPa was performed using periodic density functional theory. As the pressure increases, the lattice constants and cell volumes calculated by LDA gradually approach those obtained by GGA-PW91. It was found that the structure of DNFP is much stiffer in the *b* direction than along the *a* and *c* axes, indicating that the compressibility of the crystal is anisotropic. As the pressure increases, the band gap gradually decreases, and this decrease is more pronounced in the low-pressure range than in the high-pressure region. An analysis of the density of states showed that the electronic delocalization in DNFP gradually increases under the influence of pressure. DNFP exhibits relatively high optical activity at high pressure. As the pressure increases, the bands in the fundamental absorption region of the absorption spectrum of DNFP become more numerous and intense.

Keywords Density functional theory · 1,4-Dinitrofurazano[3,4-b]piperazine · Hydrostatic pressure · Band gap · Absorption properties

W. Wang · W. Zhu (✉) · H. Xiao
Institute for Computation in Molecular and Materials Science and Department of Chemistry, Nanjing University of Science and Technology, Nanjing 210094, China
e-mail: zhuwh@njust.edu.cn

W. Zhu
State Key Laboratory of Explosion Science and Technology, Beijing Institute of Technology, Beijing 100081, China

J. Li · B. Cheng
Institute of Chemical Materials, China Academy of Engineering Physics, Mianyang 621900, China

Introduction

Energetic nitrogen-rich heterocyclic compounds have attracted considerable attention due to their novel properties: high density, high positive heat of formation, and good thermal stability. Among these heterocyclic systems, nitraminofurazan derivatives have drawn a great deal of interest since the 1980s [1, 2]. 1,4-Dinitrofurazano[3,4-b]piperazine (DNFP) is a nitraminofurazan containing two N–NO_2 structures, a piperzine ring, and a furazan ring [3]. The furazan ring—an energetic, nitrogen-rich, heterocyclic group—presents a high enthalpy of formation, good thermal stability, and an active-oxygen-bearing cycle. A great deal of research has shown that the furazan ring is a very effective structural unit for enhancing the performance of high-energy density materials [4–7].

DNFP is a relatively insensitive energetic material; its impact sensitivity (H_{50}) is 162 cm [8]. It is more dense (1.828 $g cm^{-3}$) [3] than the commonly used explosive RDX (1,3,5-trinitro-1,3,5-triazine), and its detonation velocity and pressure are close to these of RDX [8]. Thus, it has the potential for application in propellants and explosives. Willer et al. [9, 10] used ethylenediamine as a starting material to synthesize DNFP by three-step reactions involving condensation–cyclization, dehydration, and nitrification. Bi et al. [8] synthesized DNFP through condensation–cyclization between *N*,*N*′-ditertbutyl ethylenediamine and dichloroglyoxime, dehydration, and nitrolysis. It is well known that the efficacy of chemical propellants and high-energy materials is closely linked to their solid-phase properties and their characteristics upon thermal decomposition [3]. Oyumi et al. [3, 11, 12] studied the thermal properties of DNFP and found that it has very reasonable thermal properties. However, DNFP is still not well understood at a fundamental and even practical level—it exhibits complex chemical behavior. Thus, there is a pressing need to gain a better understanding of its structure and properties.

When propellants and explosives are sufficiently excited they can undergo exothermic dissociation because these materials contain tightly bonded groups of atoms [13]. The macroscopic properties of these materials ultimately depend on their microscopic structures, such as their electronic structures. During the detonation process, DNFP experiences enormous pressure effects. Therefore, one fundamental aspect of its decomposition and burning is its structure during a high-pressure explosion. In addition, knowledge of the mechanical response of DNFP is useful for interpreting and understanding the shock-induced chemical decomposition of DNFP.

It is a challenging task to investigate the microscopic properties of energetic materials under high pressures experimentally (i.e., practically). As a complement to such experimental work, theoretical simulation provides an effective way to model the physical and chemical properties of complex solids at the atomic level. Recently, methods utilizing density functional theory (DFT) with pseudopotentials and a plane-wave basis set have become well established. Such methods have been successfully applied to study the structures and properties of energetic solids under hydrostatic compression [14, 15]. Much work has been done to investigate the synthesis of DNFP, but work studying the structural properties of DNFP with increasing pressure appears to be scarce.

In this study, we performed periodic DFT calculations to study the structural, electronic, and optical absorption properties of DNFP under hydrostatic pressures of 0–100 GPa. To investigate the crystal structure of DNFP at different pressures, atomic positions and unit-cell parameters were allowed to relax to their minimum energy configurations. Then we examined the variations in the structural and optical absorption properties of DNFP under different pressures.

The remainder of this paper is organized as follows. A brief description of our computational method is given in the second section. The results and discussion are presented in the third section, followed by a summary of our conclusions in the final section.

Computational methods

The calculations performed in this study were done within the framework of DFT based on the CASTEP code [16], using Vanderbilt-type norm-conserving pseudopotentials [17] and a plane-wave expansion of the wavefunctions. The self-consistent ground state of the system was determined by using a band-by-band conjugate gradient technique to minimize the total energy of the system with respect to the plane wave coefficients. The electronic wavefunctions were obtained using a density-mixing minimization method [18] for the self-consistent field calculation, and the structures were relaxed using the Broyden, Fletcher, Goldfarb, and Shanno (BFGS) [19] method. Geometry optimization is achieved by reducing the magnitudes of the calculated forces and stresses until they become smaller than defined convergence tolerances. Therefore, it is possible to specify an external stress tensor to model the behavior of the system under tension, compression, shear, etc. In such cases, the internal stress tensor is iterated until it becomes equal to the applied external stress. The LDA functional proposed by Ceperley and Alder [20] and parameterized by Perdew and Zunder [21] (and thus termed "CA-PZ") was employed in this work. The cutoff energy for plane waves was set to 550 eV. Brillouin zone sampling was performed using the Monkhorst–Pack scheme with a *k*-point 2×2×1 grid. The values of the kinetic energy cutoff and the *k*-point grid were chosen to ensure the convergence of the total energy.

We used the crystal structure of DNFP at ambient pressure and temperature as the input structure. DNFP crystallizes in a monoclinic lattice with the space group $P2_1/c$, and contains four $C_4H_4N_6O_5$ molecules per unit cell [3]. Figure 1 displays the atomic structures of crystalline and molecular DNGP. The experimental crystal structure of DNFP [3] was first relaxed to allow the lattice configurations, cell shape, and volume to change at ambient pressure. We then applied hydrostatic compression (in the range of 1–100 GPa) to relax the crystal structure without any symmetry constraints. All of the calculations performed in this work were based

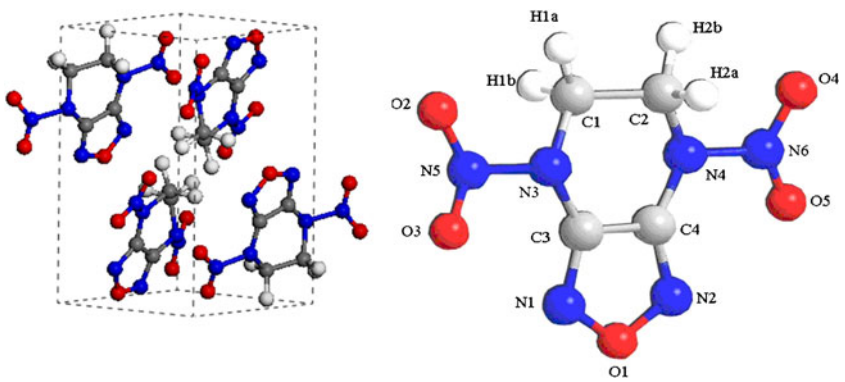

Fig. 1 Atomic structures of crystalline and molecular DNFP. *Gray*, *blue*, *red*, and *white spheres* represent C, N, O, and H atoms, respectively

Table 1 Experimental and relaxed lattice constants (Å) and angles (degrees) for crystalline DNFP

	This work				Experimental value [3]
	LDA	PBE	RPBE	PW91	
a	9.151	10.990	11.399	11.005	9.743
b	6.680	7.419	7.517	7.414	6.636
c	12.029	14.897	15.360	14.892	12.165
β	92.7°	97.7	98.6	97.7°	94.2°

on the same crystal structure of DNFP. Geometry relaxation was performed until the system converged, which meant that the total energy of the system was less than 2.0×10^{-5} eV, the residual force was less than 0.05 eV/Å, the atomic displacement was less than 0.002 Å, and the residual bulk stress was less than 0.1 GPa. Previous studies that employed the same approach to simulate the hydrostatic compression of other energetic crystals [22–24] produced results that were in agreement with those obtained experimentally.

Results and discussion

Crystal structures

We applied four different functionals to bulk DNFP at ambient conditions as a well-studied benchmark test. The LDA (CA-PZ) and the generalized gradient approximation (GGA) (PBE [25], RPBE [26], and PW91 [27]) functionals were selected to fully relax the DNFP phase without any constraint. The calculated lattice parameters are given in Table 1, together with experimental values [3]. The differences between the calculated and experimental values were found to be typical of those observed for the LDA and GGA to DFT. The errors in the LDA (CA-PZ) results were slightly smaller than those seen in the GGA (PBE, RPBE, and PW91) results when compared with the experimental values. This shows that the accuracy of LDA is better than that of GGA in predicting crystal structures. Table 2 lists the LDA-relaxed bond lengths and bond angles of crystalline DNFP at ambient conditions, together with the corresponding experimental data. The results show that the bond lengths and bond angles compare well with the experimental values. The discrepancies between the calculated and experimental values are typical of the LDA approximation to DFT. These comparisons confirm that our computational parameters are reasonable.

Figure 2 shows the effect of pressure on the lattice constants of DNFP calculated using the GGA and LDA functionals. It was found that the use of GGA and LDA lead to the same trend: the lattice constants gradually decrease as the pressure increases. Over the whole pressure range considered, the lattice constants calculated by GGA are larger than those calculated by LDA. Previous studies [28, 29] on several energetic crystals have shown that GGA generally overestimates the lattice constants while LDA underestimates them when compared to experimental data. This is consistent the results obtained in this work. To examine the pressure dependence of the lattice constants of DNFP, we fitted a quadratic of the form $a_0+a_1P+a_2P^2$ for each LDA-calculated lattice constant as function of pressure. The

Table 2 Experimental and relaxed bond lengths (Å) and bond angles (degrees) for crystalline DNFP at ambient conditions

	Experimental value [3]	Calculated in this work
Bond lengths		
C1–C2	1.496	1.505
C2–N4	1.479	1.464
N4–C4	1.387	1.375
C4–C3	1.426	1.427
C3–N3	1.388	1.376
N3–C1	1.479	1.463
N1–C3	1.295	1.311
N1–O1	1.387	1.384
O1–N2	1.388	1.378
N2–C4	1.295	1.312
N3–N5	1.389	1.404
N4–N6	1.382	1.402
N5–O2	1.215	1.221
N5–O3	1.216	1.230
N6–O4	1.221	1.229
N6–O5	1.212	1.221
Bond angles		
N3–C1–C2	109.5	109.6
C1–C2–N4	109.5	109.9
C2–N4–C4	116.0	116.8
N4–C4–C3	120.2	119.9
C4–C3–N3	120.2	120.7
C3–N3–C1	116.9	118.0
N1–C3–C4	109.7	109.4
C3–C4–N2	109.9	109.4
C4–N2–O1	103.9	104.2
N2–O1–N1	112.3	112.7
O1–N1–C3	104.0	104.1
C2–N4–N6	117.6	118.2
C1–N3–N5	117.4	117.6
N4–N6–O4	115.6	115.5
N4–N6–O5	117.4	116.8
N3–N5–O2	116.1	116.1
N3–N5–O3	117.0	116.4

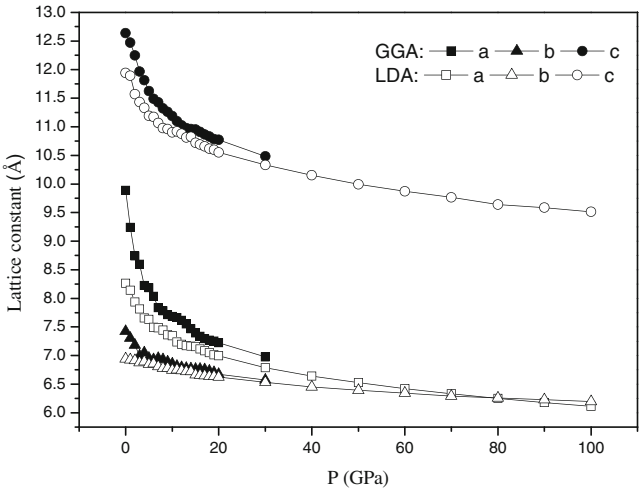

Fig. 2 Lattice constants of DNFP as a function of hydrostatic pressure

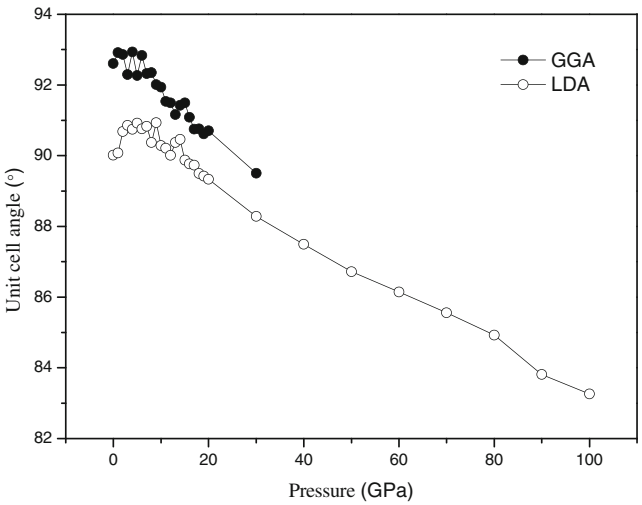

Fig. 3 Unit-cell angle β of DNFP as a function of the hydrostatic pressure

coefficients a_1 and a_2 for lattice constant a are −0.044 Å/GPa and 0.00028 Å/GPa^2, respectively. For lattice constant b, a_1 and a_2 are −0.015 Å/GPa and 0.00008 Å/GPa^2, respectively, and for lattice constant c, a_1 and a_2 are −0.049 Å/GPa and 0.00033 Å/GPa^2, respectively. This shows that the magnitudes of the quadratic coefficients a_1 and a_2 (which reflect the pressure-induced changes in the lattice constants for the a, b, and c axes) are different. The structure is much stiffer in the b direction than along the a and c axes. Therefore, the compressibility of the DNFP crystal is anisotropic. As shown in Fig. 2, the a and c axes are more compressible than the b axis. The order of compressibility for the lattice constants of the DNFP crystal is as follows: $c>a>b$. The greatest compression of the unit cell occurs for pressures of 0–10 GPa. Above that pressure range, the lattice parameters decrease slowly with increasing pressure.

Figure 3 presents the variations in the unit-cell angle β with increasing pressure, calculated using the GGA and LDA functionals. The GGA and LDA results show the same trend for the unit-cell angle β: it decreases slowly with increasing pressure. The decrease in β is more irregular in the high-pressure region than in the low-pressure region. The unit-cell angles α and γ are 90°; they remain unchanged over the entire pressure range from 0 to 100 GPa (not shown in Fig. 3). The observed lack of continuous behavior in Fig. 3 may be due to numerical fluctuations.

The effect of pressure on the unit-cell volume, as calculated using LDA and GGA, is presented in Fig. 4. We can see from Fig. 4 that the GGA and LDA results show the same trend: as the pressure increases, the volume decreases monotonically. Up to 70 GPa, the volume compression is 50 %. At a given pressure, the unit-cell volume estimated by LDA is lower than that estimated by GGA. This is consistent with previous DFT studies on several energetic solids [29, 30]. The two curves are also closer together in the high-pressure region, implying that the DFT calculations performed for high pressures may be more reliable (due to the enhanced intermolecular interactions at such pressures). Since conventional formulations of DFT do not include dispersion interactions, DFT appears to be inadequate for studies of organic molecular crystals that are weakly bonded by van der Waals forces at low pressures. However, there is evidence that DFT can be used to treat weakly bound molecular systems under sufficient degrees of compression [30]. Our previous calculations also show that DFT can accurately describe the intermolecular interactions that occur in HMX [29] and HNS crystals [12] subjected to high pressures. Since the LDA results present the same trend as the GGA ones, the LDA functional was used in subsequent calculations.

The crystal packing of the DNFP molecule is quite efficient. We performed statistical averaging of the lengths of different bonds in DNFP (obtained using LDA) to investigate the effect of pressure on them. Figure 5 displays the

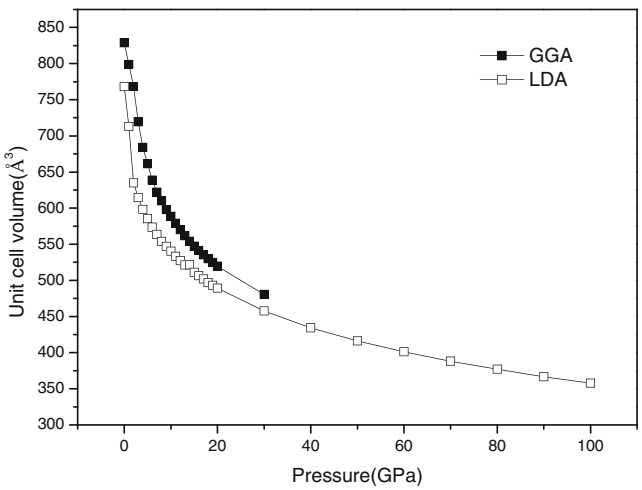

Fig. 4 Unit-cell volume of DNFP as a function of hydrostatic pressure

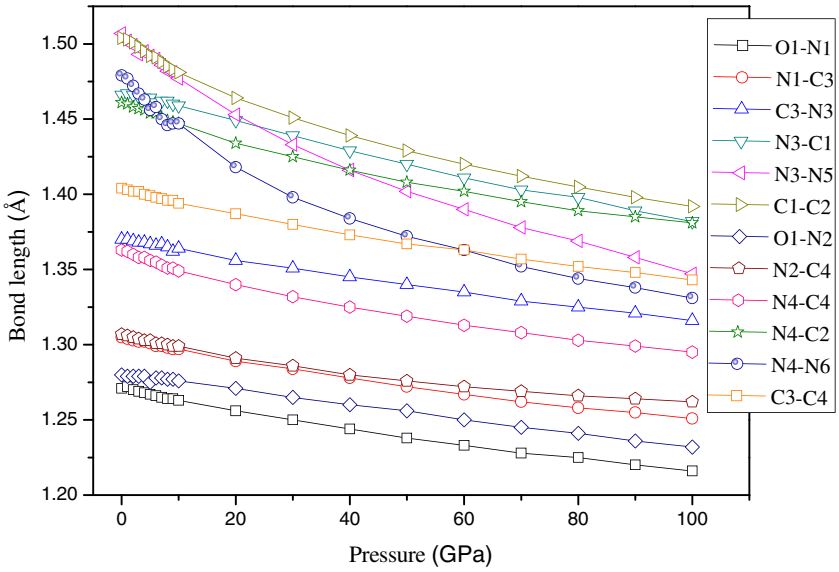

Fig. 5 Bond lengths of DNFP as a function of hydrostatic pressure

bond lengths in DNFP at different pressures. It is clear that the bond lengths in DNFP gradually decrease under the influence of pressure, although the lengths of the bonds N3–N5 and N4–N6 decrease more than those of the other bonds with increasing pressure. This means that the two bonds N3–N5 and N4–N6 are easier to weaken than other bonds under compression. We can therefore infer that the trigger linkage in DNFP is N–NO_2, while the other bonds are relatively strong and resistant to rupture. This is supported by experimental data [3].

Electronic structures

Figure 6 displays the effect of pressure on the band gap of DNFP, as calculated using GGA and LDA. As the pressure increases, the band gap gradually decreases without any significant discontinuity. This is because the decrease in intermolecular space under compression leads to an increase in the overlaps among different groups of bands, and hence increased charge overlap and delocalization in the system. However, the average decrease in the band gap varies depending on the pressure range. When linear fits are performed in different pressure ranges, the average decrease in the band gap up to 10 GPa is 0.0511 eV/GPa, while it is 0.0336 eV/GPa from 10 to 50 GPa and 0.0057 eV/GPa from 50 to 100 GPa. This indicates that the decrease in energy is more pronounced in the low-pressure range compared to the high-pressure region, which is in agreement with previous theoretical studies on HNS [12], AP [24], anthracene [31], and nitromethane [23, 28] subjected to high pressures. For 50 % compression (P= 70 GPa), the band gap drops from 3.17 eV at ambient pressure to 1.67 eV. In the pressure region 0–20 GPa, the decrease in the band gap is 0.86 eV. This value is larger than the pressure-induced band-gap reduction of 0.23 eV calculated for nitromethane [28] using DFT for pressures up to 20 GPa, and the calculated reduction of about 0.63 eV in anthracene [31] up to 10 GPa, which was obtained using DFT-LDA. In addition, Fig. 6 indicates that there is no significant change in the band gap in the vicinity of the pressure 34 GPa, which is close to the detonation pressure of DNFP determined experimentally [32]. This shows that compressing the crystal DNFP to a pressure that is an order of magnitude higher than that observed in developed detonation waves does not lower the band gap enough to provide a significant thermal population of conduction electrons at detonation temperatures. Previous theoretical studies on HNS [12], nitromethane [28], HMX [29], RDX [33], and lead azide [34] have shown that these materials also present some band gap lowering under compression to the densities associated with detonation, but not enough to produce a significant population of excited states at detonation temperatures. These observations agree qualitatively with our results here.

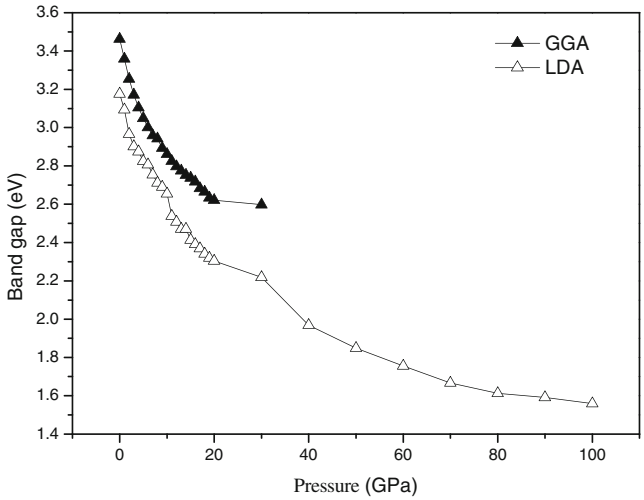

Fig. 6 Band gap of DNFP as a function of hydrostatic pressure

The calculated total density of states (DOS) and the partial DOS (PDOS) of the DNFP crystal are displayed in Fig. 7 for various pressures. As the pressure increases, the DOS peaks in the valence bands become more and more dispersed, and they tend to shift to lower energy. This shows that the electronic delocalization in DNFP gradually increases under the influence of hydrostatic pressure. In the upper valence band, DNFP has a relative sharp peak near the Fermi level at 0 GPa, indicating that the top valence bands of the band structure are flat. As the pressure increases further, the sharp peak becomes increasingly smooth. This means that the band splitting and band dispersion increase, and the DOS broadens. This may be because the intermolecular distances are reduced, so the intermolecular interactions strengthen with increasing pressure. Upon compression, the DOS peaks in the conduction bands have a tendency to shift to lower energies. This leads to a reduction in the gap between the conduction and valence bands. It can be inferred from Fig. 6 that the band gap closes in DNFP

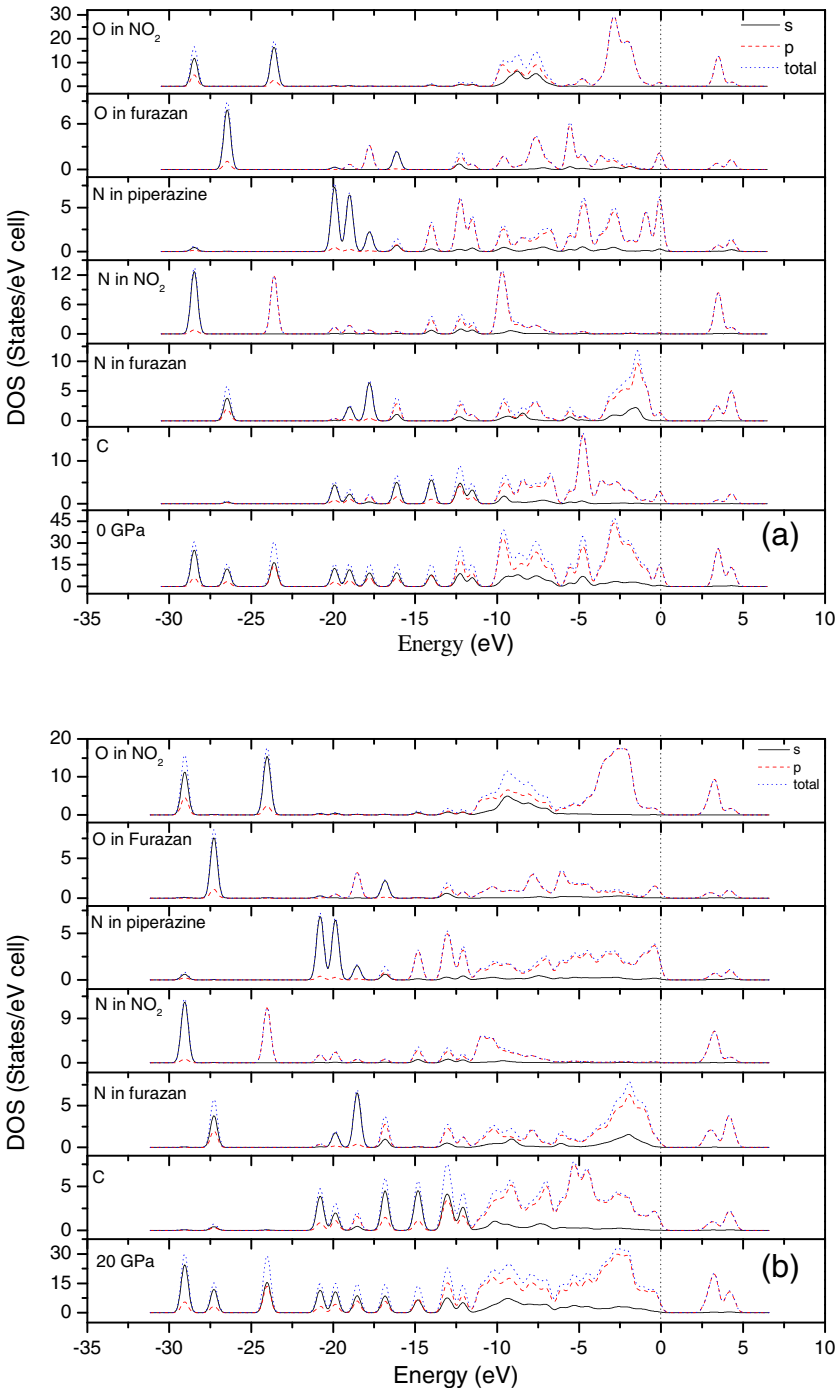

Fig. 7a–d Total and partial density of states (DOS) for the O states in NO_2, O states in the furazan ring, N states in the piperazine ring, N states in NO_2, C states, and DNFP at pressures of **a** 0 GPa, **b** 20 GPa, **c** 60 GPa, and **d** 100 GPa. The Fermi energy is shown as a *vertical dashed line*

Fig. 7a–d (continued)

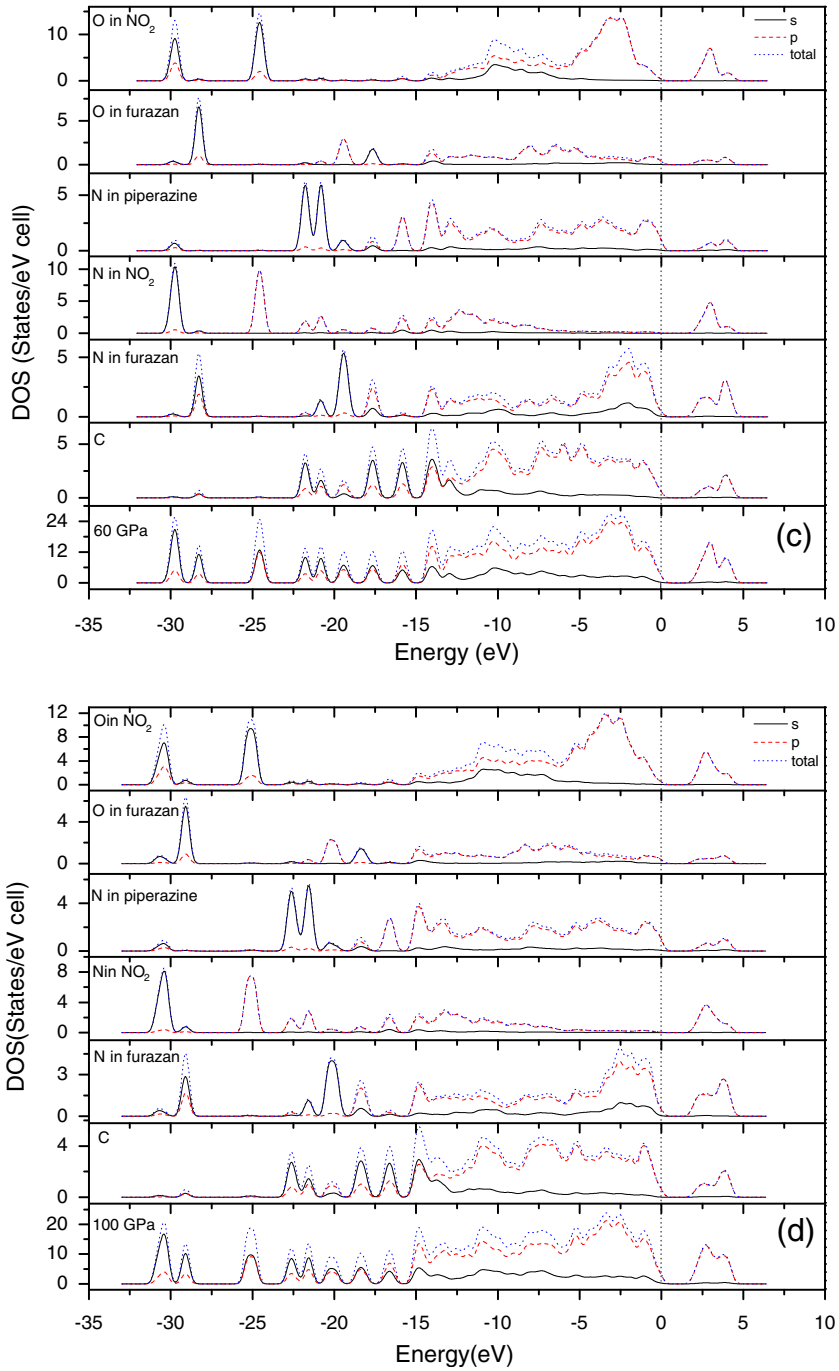

under compression, and that DNFP has metallic properties. Gilman [35, 36] has proposed that metallization occurs at the shock front due to the bending of covalent bonds. Such metallization has been also been found to occur under hydrostatic compression in the covalently bonded energetic material nitromethane [28]. These conclusions support our findings here. At low pressure, the DOS from −15 eV up to the Fermi level is dominated by the *p* states, while it is dominated by the *s* and *p* states at high pressure. This indicates that there is an increase in charge overlap in the system with increasing pressure.

The atom-resolved DOS and PDOS of DNFP at different pressures are also shown in Fig. 7. As the pressure increases, the DOS peaks of the N states in the piperazine ring, the N states in NO_2, the N states in the furazan ring, the C states, the O states in the furazan ring, and the O states in NO_2 in the valence bands become more and more dispersed, and those in the conduction bands have a tendency to shift to lower energy. This shows that crystal compression greatly increases the likelihood of electronic excitations. In the upper valence bands from −10 to 0 eV, compression moves the N states in the piperazine ring toward the Fermi level,

and several of the main peaks relating to those states merge together. Also, the states of N in the piperazine ring contribute more to the upper valence bands than the other atoms. This shows that the N in the piperazine ring acts as an active center. Thus, the electrons from the N states in the piperazine ring become more and more excited under compression. This implies that N–NO_2 bond fission may be favorable in the decomposition of crystalline DNFP. These results show that compressing the DNFP crystal increases the probability of N–NO_2 bond fission. This is in agreement with experimental results on the thermal decomposition mechanisms of DNFP [3, 8]. In addition, in the upper valence bands from −10 to 0 eV, compression moves the C states and N states in the furazan ring toward the Fermi level, and several of the main peaks relating to these states merge together. This indicates that the electrons from the C states and N states in furazan become more and more excited under compression. This indicates that the furazan ring may decompose and produce some small gas molecules, which again is in agreement with experimental data [3].

Finally, we tried to correlate the stability (or explosive character) of DNFP under compression with its electronic structure. The electronic structure of a solid is intimately related to its fundamental physical and chemical properties. The band gap is an important feature of the electronic structure of a material. Xiao et al. [37, 38] used the semi-empirical discrete variational Xα (DV-Xα) and extended Hückel–crystal orbital (EH-CO) methods to study the band structure of metal azides, and found that the energy gap between the HOCO and LUCO (the highest occupied crystal orbital and the lowest unoccupied crystal orbital) was correlated with the corresponding impact sensitivity. Since then, many theoretical studies of the polymorphs of HMX [29], alkali metal azides [34, 39], heavy-metal azides [40, 41], nitroanilines [14], and K-doped cuprous azides [42] performed within the framework of periodic DFT have also confirmed this relationship between the band gap and impact sensitivity. Gilman [35, 36] has emphasized the role of HOMO–LUMO gap closure in the explosion of molecules suffering shear strain and shocks. Luty et al. [43] reported that band gap closure is related to the stability of the material. Further, investigations on the excitonic mechanism of detonation initiation [44, 45] have shown that the pressure inside the impact wavefront reduces the band gaps between valence and conduction bands and can promote the HOMO–LUMO transition within a molecule. These studies suggest that the band gap in gas molecules undergoing shear strain, impact waves, or distortion relates directly to the sensitivity. Our previous studies [46, 47] derived a first-principles band-gap criterion to measure impact sensitivity for a series of energetic crystals. For energetic crystals that have a similar structure and thermal decomposition mechanism, the smaller the band gap, the easier it is to transfer an electron from the valence band to the conduction band, and the more the material decomposes and explodes. As can be seen in Fig. 6, the band gap of the DNFP crystal gradually decreases as the pressure increases. Therefore, it may be inferred that the impact sensitivity for DNFP increases with rising pressure. This is in agreement with numerous experimental observations that applying pressure increases the sensitivity of explosives to detonation initiation [48].

Optical absorption spectra

In this section, we describe our investigation of the optical absorption coefficients of the DNFP crystal at different pressures. The interaction of a photon with the electrons in a system can result in transitions between occupied and unoccupied states. The spectrum resulting from these excitations can be described as a joint density of states between the valence and conduction bands. The imaginary part $\varepsilon_2(\omega)$ of the dielectric function can be obtained from the momentum matrix elements between the occupied and unoccupied wavefunctions within the selection rules, and the real part $\varepsilon_1(\omega)$ of the dielectric function can be calculated from the imaginary part $\varepsilon_2(\omega)$ by the Kramer–Kronig relationship. The absorption coefficient $\alpha(\omega)$ can be evaluated from $\varepsilon_1(\omega)$ and $\varepsilon_2(\omega)$ [49].

$$\alpha(\omega) = \sqrt{2}\omega\left(\sqrt{\varepsilon_1^2(\omega) + \varepsilon_2^2(\omega)} - \varepsilon_1(\omega)\right)^{1/2} \quad (1)$$

The absorption coefficients $\alpha(\omega)$ of DNFP at different pressures are shown in Fig. 8. The absorption spectrum is active in various regions corresponding to the molecular or

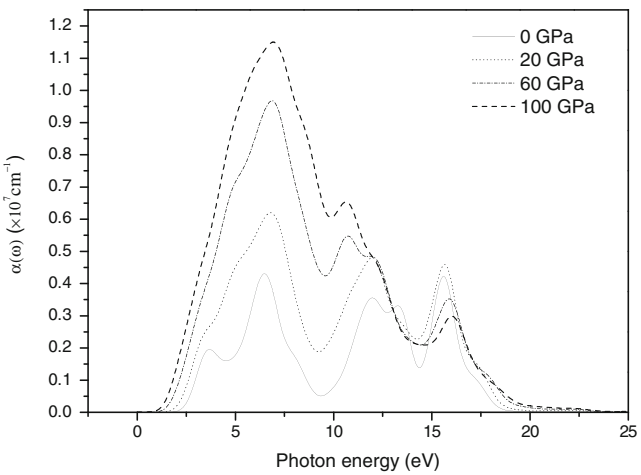

Fig. 8 Optical absorption spectrum of DNFP at different hydrostatic pressures

lattice structures of the individual materials. The absorption spectrum of DNFP has a qualitatively similar appearance at different pressures. There is an absorption band from 0 to 25.0 eV and strong optical absorption from 2.5 to 17.5 eV. The magnitudes of the absorption coefficients of these peaks allow optical transitions due to excitons. At ambient pressure, DNFP exhibits a relatively high absorption coefficient over a few closely spaced bands. The absorption bands from 2.5 to 4.4 eV and 14.3 to 16.8 eV correspond to the frequency of C–H stretching. The bands in the range 5.1–12.6 eV overlap, forming the strongest absorption region, which corresponds to N–O vibrations and ring distortion. The peak at 13.3 eV corresponds to C=N stretching. As the pressure increases, the absorption peak of DNFP becomes wider and taller. This suggests that DNFP has relatively high optical activity at high pressure. In addition, DNFP exhibits higher absorption coefficients at high pressure than at low pressure in the frequency range 0–12.5 eV, indicating a shift toward higher frequencies in the absorption spectra. The results calculated here indicate that the bands in the fundamental absorption region of the absorption spectrum of DNFP are more numerous and intense at high pressure than at low pressure.

Conclusions

In this work, we performed a systematic theoretical study of the structural, electronic, and optical absorption properties of crystalline DNFP under hydrostatic pressures of 0–100 GPa using density functional theory. The results show that the structure of DNFP is much stiffer in the *b* direction than along the *a* and *c* axes, indicating that the compressibility of the crystal is anisotropic. As the pressure increases, the band gap gradually decreases, and this decrease is more pronounced in the low-pressure range than in the high-pressure region. An analysis of the density of states shows that electronic delocalization gradually increases in DNFP under the influence of pressure. Our improved understanding of the stability of DNFP under compression, obtained by studying DNFP's electronic structure, indicates that applying pressure increases the impact sensitivity of DNFP to detonation initiation. As the pressure increases, DNFP presents increasingly high optical activity. The bands in the fundamental absorption region of the absorption spectrum of DNFP are more numerous and intense at high pressure than at low pressure.

Acknowledgments This work was supported by the NSAF Foundation of National Natural Science Foundation of China and the China Academy of Engineering Physics (grant no. 10876013), the Opening Project of the State Key Laboratory of Explosion Science and Technology (Beijing Institute of Technology; KFJJ10-13M), and NUST Research Funding (no. 2011YBXM08).

References

1. Cichra DA, Holden JR, Dickinson C (1980) Estimation of "normal" densities of organic explosives from empirical atomic volumes (NSWC TR 79–273). Naval Surface Warfare Center (White Oak), Silver Spring, MD
2. Rothstein LR, Petersen R (1979) Propellants Explos 4:56–60
3. Oyumi Y, Rheingold AL, Brill TB (1985) J Phys Chem 90:4686–4690
4. Ronald A (2004) Advanced energetic materials. National Academies Press, Washington, DC
5. Fried LE, Manaa MR, Pagoria PF, Simpson RL (2001) Annu Rev Mater Res 31:291–321
6. Zhang DX, Zhang Y, Wang Q (2004) J Solid Rocket Technol 27:32–36
7. Yan QL, Li XJ, Ji YP (2008) Chem Propellants Poly Mater 6:27–33
8. Bi FQ, Wang BZ, Wang XJ (2009) Chin J Energ Mater 17:537–540
9. Willer RL, Moore DW (1985) J Org Chem 50:5123–5127
10. Willer RL, Ridgecrest CA (1985) US Patent 4539405
11. Oyumi Y, Brill TB (1987) J Combust Flame 68:209–216
12. Oyumi Y, Brill TB (1987) J Thermochim Acta 116:125–130
13. Zhu WH, Shi CH, Xiao HM (2009) J Mol Struct (THEOCHEM) 910:148–153
14. Zhu WH, Zhang XW, Wei T, Xiao HM (2009) J Mol Struct (THEOCHEM) 910:84–89
15. Zhu WH, Xiao HM (2007) J Solid State Chem 180:3521–3528
16. Segall MD, Lindan PJD, Probert MJ, Pickard CJ, Hasnip PJ, Clark SJ, Payne MC (2002) J Phys Condens Matter 14:2717–2744
17. Vanderbilt D (1990) Phys Rev B 41:7892–7895
18. Kresse G, Furthmüller J (1996) Phys Rev B 54:11169–11186
19. Fletcher R (1980) Practical methods of optimization, vol 1. Wiley, New York
20. Ceperley DM, Alder BJ (1980) Phys Rev Lett 45:566–569
21. Perdew JP, Zunger A (1981) Phys Rev B 23:5048–5079
22. Xu XJ, Zhu WH, Xiao HM (2007) J Phys Chem B 111:2090–2097
23. Liu H, Zhao JJ, Wei DQ, Gong ZZ (2006) J Chem Phys 124:124501
24. Zhu WH, Zhang XW, Zhu W, Xiao HM (2008) Phys Chem Chem Phys 10:7318–7323
25. Perdew JP, Burke K, Ernzerhof M (1996) Phys Rev Lett 77:3865–3868
26. Hammer B, Hansen LB, Norskov JK (1999) Phys Rev B 59:7413–7421
27. Perdew JP, Chevary JA, Vosko SH, Jackson KA, Pederson MR, Singh DJ, Fiolhais C (1992) Phys Rev B 46:6671–6678
28. Reed EJ, Joannopoulos JD, Fried LE (2000) Phys Rev B 62:16500
29. Zhu WH, Zhang XW, Wei T, Xiao HM (2009) Theor Chem Accounts 124:179–186
30. Byrd EFC, Rice BM (2007) J Phys Chem C 111:2787–2796
31. Hummer K, Puschnig P, Ambrosch-Draxl C (2003) Phys Rev B 67:184105–184105
32. Willer RL, Calif R (1985) US Patent 4539405
33. Kuklja MM, Kunz AB (1999) J Appl Phys 86:4428–4434
34. Younk EH, Kunz AB (1997) Int J Quantum Chem 63:615–620
35. Gilman JJ (1995) Philos Magn B 71:1057–1068
36. Gilman JJ (1993) Philos Magn B 67:207–214
37. Xiao HM, Li YF, Qian JJ (1994) Acta Phys Chim Sin 10:235–240
38. Xiao HM, Li YF (1995) Sci Chin B 38:538–545
39. Zhu WH, Xiao JJ, Xiao HM (2006) Chem Phys Lett 422:117–121
40. Zhu WH, Xiao HM (2006) J Phys Chem B 110:18196–18203
41. Zhu WH, Xiao HM (2008) J Comput Chem 29:176–184
42. Zhu WH, Zhang XW, Wei T, Xiao HM (2008) Chin J Chem 26:2145–2149

43. Luty T, Ordon P, Eckhardt CJ (2002) J Chem Phys 117:1775–1786
44. Kuklja MM, Stefanovich EV, Kunz AB (2000) J Chem Phys 112:3417–3423
45. Kuklja MM, Kunz AB (2000) J Appl Phys 87:2215–2218
46. Zhu WH, Xiao HM (2010) Struct Chem 21:657–665
47. Zhu WH, Xiao JJ, Ji GF, Zhao F, Xiao HM (2007) J Phys Chem B 111:12715–12722
48. Botcher TR, Landouceur HD, Russel TR (1998) Shock compression of condensed matter—1997. In: Schmidt SC, Dandekar DP, Forbes JW (eds) Proc APS topical group. AIP, Woodbury
49. Saha S, Sinha TP, Mookerjee A (2000) Phys Rev B 62:8828–8834